Published in final edited form as:

Proc IEEE Int Symp Biomed Imaging. 2013 April ; 2013: 390–393. doi:10.1109/ISBI.2013.6556494.

A NEW ALGORITHM FOR TRABECULAR BONE THICKNESS COMPUTATION AT LOW RESOLUTION ACHIEVED UNDER IN VIVO CONDITION

Yinxiao Liu[1], **Dakai Jin**[1], and **Punam K. Saha**[1,2]

[1]Department of ECE, University of Iowa, Iowa City, IA, 52242

[2]Department of Radiology, University of Iowa, Iowa City, IA, 52242

Abstract

Adult bone diseases, especially osteoporosis, lead to increased risk of fracture associated with substantial morbidity, mortality, and financial costs. Clinically, osteoporosis is defined by low bone mineral density (BMD); however, increasing evidence suggests that the micro-architectural quality of trabecular bone (TB) is an important determinant of bone strength and fracture risk. Accurate measurement of trabecular thickness and marrow spacing is of significant interest for early diagnosis of osteoporosis or treatment effects. Here, we present a new robust algorithm for computing TB thickness and marrow spacing at a low resolution achievable *in vivo*. The method uses a star-line tracing technique that effectively deals with partial voluming effects of *in vivo* imaging where voxel size is comparable to TB thickness. Experimental results on cadaveric ankle specimens have demonstrated the algorithm's robustness (ICC>0.98) under repeat scans of multi-row detector computed tomography (MD-CT) imaging. It has been observed in experimental results that TB thickness and marrow spacing measures as computed by the new algorithm have strong association ($R^2 \in \{0.85, 0.87\}$) with TB's experimental mechanical strength measures.

Index Terms

Trabecular bone thickness; marrow spacing; star line tracing; multi-row detector CT; bone biomechanics

1. INTRODUCTION

Adult bone diseases, especially osteoporosis, lead to increased risk of fracture associated with substantial morbidity, mortality, and financial costs [1]. Approximately, 30% of postmenopausal white women in the United States suffer from osteoporosis [2] and the prevalence in Europe and Asia is similar. Clinically, osteoporosis is defined by low bone mineral density (BMD) [1]. However, increasing evidence suggests that micro-architectural quality of trabecular bone (TB) is an important determinant of bone strength and fracture risk [3–6]. Trabecular bone or spongy bone form a dense network of bone plates and rods and it dominates in the vertebrae and at locations near the joints of long bones (metaphysis and epiphysis). Bone atrophy as it occurs in osteoporosis, leads to either homogeneous or heterogeneous thinning of the trabecular elements. Besides changes in TB network connectivity and topology, TB thickness and marrow spacing between trabeculae play

critical roles in determining the mechanical competence of bone and thus resistance to osteoporotic fractures [7]. Thus an accurate and robust *in vivo* method for computing TB thickness and marrow spacing measures is of significant interest in osteoporosis imaging research.

The classical approach of measuring trabecular thickness is based on histomorphometry of transiliac bone biopsies [8]. The emergence of imaging technologies such as micro computed tomography (μ-CT) [9] enables reconstruction of high resolution three-dimensional (3-D) images calling for more elaborate techniques for computing TB thickness. Recently, *in vivo* multi-row detector CT (MD-CT) has become a promising modality for high quality TB imaging at peripheral sites [10–12] that avoids the problems of invasive bone biopsies. Therefore, an accurate and robust measure of TB thickness and marrow spacing that may be computed via *in vivo* MD-CT imaging would be useful as an effective indicator of quantitative bone quality for clinical trials evaluating fracture risks under different clinical conditions.

Several methods have been reported [13–16] toward computing TB thickness and marrows spacing. Hildebrand *et al.* [13] presented a model-independent binary approach involving inscribing spheres into the target TB structure where trabecular thickness at any location is computed as the diameter of the largest inscribed sphere containing that location. This approach is well suited for high-resolution images that can easily be segmented but is bound to fail when significant partial voluming is present. Saha *et al.* [14] overcome this issues of partial voluming at low resolution in TB thickness computation by introducing the use of fuzzy distance transform. Star volume has been developed and used as the method for TB marrow spacing measure [15] [16]. It is defined as the mean volume of all parts of an object that can be seen un-obscured from a random point within the target object.

Here, we introduce a star-line based algorithm for an accurate and robust measure of TB thickness and marrow spacing at *in vivo* resolution in the presence of significant partial voluming. Reproducibility of the method is examined under repeat scan MD-CT imaging and under random changes in skeletal point locations. Finally, the ability of the two MD-CT derived measures to predict TB's experimental strengths are evaluated and the results are presented.

2. ALGORITHMS AND METHODS

The new thickness computation method is applicable to a fuzzy representation of any object where the membership value at an image voxel is interpreted as partial occupancy of the target object within the voxel or the local object density. Depending on the current application, the algorithm will be applied on TB bone images where the value at a voxel p represents the bone volume fraction (BVF) at that voxel and it is denoted as (p). MD-CT imaging acquires data in the Hounsfield unit and these numbers are converted to BVF measures using average MD-CT values in three calibration rods in the INTable™ phantom. The Calibration Phantom contains concentrations of 0, 75 and 150 mg/cm^3 of calcium hydroxyapatite homogeneously (CaHA) blended into the CT-Water™ compound. The

marrow spacing between individual trabeculae is computed from marrow volume fraction image (MVF) derived from BVF as:

$$\mathrm{MVF}\,(p) = 1.0 - \mathrm{BVF}\;(p)\,.$$

In the following, first, we present the theory and algorithm for thickness computation followed by description of different TB measures and experimental plans and methods.

2.1. Theory and algorithms

The new thickness computation method consists of two major modules – (1) computation of local thickness at axial points and (2) inheritance of local thickness value at a non-axial point from the nearest axial point. Let us consider a binary *object* $O \subset R^3$. A point $p \subset O$ is an *axial point* in O if there is a maximally included *ball* of O that is centered at p. At an *axial point* $p \in O$, the *thickness* of O at p is the diameter of the maximally included *ball* of O centered at p [17]; let us denote the ball as $B_{\max}(p)$ and its diameter as $d_{\max}(p)$. Now, consider all possible intercepts of O that pass through the *axial point* p; denoted as $\Pi_o(p)$. It may be shown that the following theorem is true and the premise of our thickness computation is built on this theorem:

Theorem 1—The diameter of the maximally included ball $B_{\max}(p)$ in O centered at an axial point p is equal to the length of the shortest intercept of O passing through p, i.e.,

$$d_{max}\,(p) = min_{\pi \in \Pi o(p)}\,|\pi|\,.$$

The new algorithm is designed to achieve an approximate measure of the term $min_{\pi \in \Pi o(p)}\,|\pi|$ in the above equation and it is solved using a star-line tracing approach. It may be noted that the above theorem is true for axial points only. Therefore, the thickness values are directly computed at axial points using a star-line approach and then these values are propagated to non-axial points using a nearest neighbor feature propagation algorithm [18].

The star-line based thickness computation algorithm is performed by locally tracing an object along m pairs of mutually opposite sample lines emanating from a candidate point . These sample lines are selected at a pseudo uniform distribution over the entire 3-D angular space [19]. For all experiments reported in this paper, we used 89 pairs of sample lines at an approximate angular separation of 15° between every two neighboring sample lines. The extent of the target fuzzy object (BVF representation of TB network for the current application) along an individual sample line is determined by integrating object membership values (here, BVF) at sample points along the specific sample line until the sample line enters into background, i.e. the object membership at the last sample point reaches to the value of zero. The local extent of the object along each sample line is recorded (Figure 1a). For each pair of opposite sample lines, local intercept length for the target object along the specific direction is determined by adding the object extent lengths along the two opposite directions. So far, the method provides m possible object intercept lengths along the m

different directions of sample line pairs. Finally, following Theorem 1, thickness of the target object at the candidate point p (red dot in Figure 1a) is computed at the shortest (orange line segment in Figure 1a) among the m different object intercept lengths along different directions. Once, the thickness values are computed at all axial locations, i.e., skeletal points [18] using the above algorithm, thickness values at non-axial points are inherited from the nearest axial points using the feature propagation algorithm introduced in [18]. Trabecular bone thickness value at a given point p is denoted as $TH_B(p)$. The thickness computation algorithm may be summarized in the following three steps:

Step 1 Computation of the surface skeleton S [18] for the TB structure B, where B is set of all voxels with nonzero BVF value.

Step 2 Computation of TB thickness $TH_B(p)$ at all skeletal points $p \in S$ using the star-line based algorithm described above.

Step 3 Computation of TB thickness $TH_B(p)$ at all non-skeletal points $p \in 0\text{-}S$ by inheriting the local TB thickness $TH_B(p)$ from the nearest skeletal voxel [18].

In the above algorithm, Step 1 is accomplished using the surface skeletonization algorithm by Saha *et al.* [18, 20]. Step 2 is accomplished as described above while the feature propagation in Step 3 is accomplished using the classical algorithm introduced in [18].

Computation of marrow spacing $SP_M(p)$ between individual trabeculae (Figure 1b) is performed using the same algorithm except that marrow volume fraction or MVF map is used instead of BVF map. Finally, two TB measures, namely, TB thickness (TH_B) and marrow spacing (SP_M) are computed over a target volume-of-interest (VOI) as follows:

$$\text{TB thickness: } TH_B = \sum_{p \in V} TH_B(p) / \|V\|, \text{ and}$$
$$\text{Marrow spacing: } SP_M = \sum_{p \in V} SP_M(p) / \|V\|.$$

Besides the two TB micro-architectural measures, average BMD over the VOI V was computed as described in [18].

2.4. Experimental plans and methods

Experiments were designed to examine – (1) accuracy, (2) reproducibility, and (3) ability of the new TB thickness and marrows measures to predict TB strength. All experiments were performed on 15 fresh-frozen human cadaveric ankle specimens harvested from 11 body donors under the Deeded Body Program at the University of Iowa. The following sequential steps were applied on each specimen – (1) MD-CT imaging, (2) image processing, and (3) mechanical testing. All ankle specimens were kept frozen until the performance of MD-CT imaging.

High resolution MD-CT scans of distal tibia were acquired at the Iowa Comprehensive Lung Imaging center, University of Iowa on a 128 slice SOMATOM Definition Flash scanner at 120 kV, 200 effective mAs, and reconstructed at 0.2 mm slice thickness using a U70u kernel achieving high spatial resolution. Three repeat MD-CT scans of each distal tibia specimen were acquired after repositioning the specimen on CT table before each scan.

TB MD-CT images were converted into BVF images using the INTable™ Calibration Phantom as discussed earlier and were resampled at 150 μm isotropic voxel. These resampled BVF images were used for computation of average BMD, TH_B, and SP_M over a target VOI.

To determine TB strength, a cylindrical TB core with 8 mm in diameter and 20.9 ± 3.3 mm in length was cored from distal tibia in situ along the proximal-distal direction. Each TB core was mechanically tested in compression using an electromechanical materials testing machine. To minimize specimen end effects, strain was measured with a 6 mm gage length extensometer attached directly to the midsection of the bone. A compressive preload of 10 N was applied and strains then set to zero. At a strain rate of 0.005 sec^{-1}, each specimen was preconditioned to a low strain with at least ten cycles and then loaded to failure. Yield stress was determined as the intersection of the stress-strain curve and a 0.2% strain offset of the modulus.

3. EXPERIMENTAL RESULTS

Results of TB thickness measures for three specimens with different experimental mechanical strengths are shown in Figure 2. An 8% difference in BMD from the strong bone (a) to the weak bone (c) leads to a 70% loss in bone strength and manifests into 20% reduction in TB thickness while 42% increase in marrow spacing measure. This observation supports that TB thickness and marrow spacing are highly sensitivity to bone degeneration.

3.1. Robustness analysis

Two different experiments were under taken to assess the robustness of the new method. The first experiment was designed to examine robustness of the method under errors in skeletal location. For this purpose, each computed skeletal voxel [18] was randomly replaced by its 3×3×3 neighbor and then Steps 2 and 3 of thickness computation algorithm were followed. Under this experiment each image points is considered as a test instance generated from MD-CT images of fifteen ankle specimens. The mean and standard deviation of errors in TB thickness computation was 8% and 6%, respectively. The mean error was reduced to 3% when average thickness value over 1 mm^3 was used.

The second experiment was conducted to examine repeat MD-CT scan reproducibility of the method. Figure 3 illustrates color-coded TB thickness map over a matching volume in three repeat MD-CT-scan data of distal tibia. For quantitative analyses, ten spherical VOIs of same radius were randomly selected in the first MD-CT scan of each specimen above the position 8 mm proximal to the distal endplate leading to a total of 150 VOIs. Post-registration algorithm was used to locate the matching VOIs in the second and third repeat scan data. It is obvious that the result of reproducibility analysis depends on the scale of VOI with larger VOI showing better reproducibility. In order to find out the relationship between the reproducibility performance and the scale of VOI, 11 different sizes of VOI in diameter were used for our experiment and the results are presented in Figure 4. It is observed in the figure that at a VOI diameter of 3.45 mm or greater, the intra-class correlation coefficient (ICC) exceeded the value of 0.95 suggesting that the measure is highly robust for assessing regional bone alteration.

3.2. Predicting bone strength

In order to examine the ability of TB thickness and marrow spacing computed by the new method to predict bone strength, a linear correlation analysis between each of the two measures and the TB's experimental yield stress was performed. The image-based measures were computed over a cylindrical VOI with its axis aligned to that of distal tibia and its length and position were selected as per the data recorded during specimen preparation and mechanical testing. The results of correlation analysis between yield stress and each of the two TB measures are shown in Figure 5. The R^2 value of of the linear correlation between BMD and TB yield stress was observed as 0.79. Both TB thickness and marrow spacing measures have demonstrated better strength to predict TB's yield stress as compared to BMD.

4. CONCLUSION

In this paper, we have presented a new thickness computation algorithm for fuzzy digital objects and have investigated its role in computing TB thickness and marrow spacing measures through MD-CT imaging under an *in vivo* condition. Results of a comprehensive study on fifteen cadaveric ankle specimens evaluating the new method are presented. Observed results have demonstrated satisfactory repeat scan reproducibility of method. TB thickness and marrow spacing measures have demonstrated higher ability to predict trabecular bone's experimental mechanical properties under an *in vivo* condition. Currently, we are investigating the role of the new method in characterizing different groups of human subjects with different clinical status of bone health.

References

1. Boonen S, Singer AJ. Osteoporosis management: impact of fracture type on cost and quality of life in patients at risk for fracture I. Curr Med Res Opin. 2008; 24:8.
2. Melton, Lr. Epidemiology of spinal osteoporosis. Spine. 1997; 22:2–11.
3. Benito M, et al. Deterioration of trabecular architecture in hypogonadal men. J Clin Endocrinol Metab. 2003; 88:1497–1502. [PubMed: 12679429]
4. Kleerekoper M, et al. The role of threedimensional trabecular microstructure in the pathogenesis of vertebral compression fractures. Calcified Tissue International. 1985; 37:594–597. [PubMed: 3937580]
5. Wehrli FW, et al. In vivo magnetic resonance detects rapid remodeling changes in the topology of the trabecular bone network after menopause and the protective effect of estradiol. J Bone Miner Res. 2008; 23:730–40. [PubMed: 18251704]
6. Wehrli FW, et al. Role of magnetic resonance for assessing structure and function of trabecular bone. Topics in Magnetic Resonance Imaging. 2002; 13:335–356. [PubMed: 12464746]
7. PARFITT AM, et al. Relationships between Surface, Volume, and Thickness of Iliac Trabecular Bone in Aging and in Osteoporosis. J Clin Invest. 1983; 72:1396–1409. [PubMed: 6630513]
8. Chavassieux, P., et al. Clinical use of bone biopsy. Vol. 2. New York: Academic Press; 2001.
9. Rüegsegger P, et al. A microtomographic system for the nondestructive evaluation of bone architecture. Calcif Tissue Int. 1996; 58:29–24.
10. Ito M, et al. Multi-Detector Row CT Imaging of Vertebral Microstructure for Evaluation of Fracture Risk. J Bone Miner Res. 2005; 20:1828–1836. [PubMed: 16160740]
11. Saha, PK., et al. Trabecular bone structural analysis using 64 multi-detector CT scanner; 29th Annual Meeting of the American Society for Bone and Mineral Research; Honolulu, HI. 2007. p. 193

12. Diederichs G, et al. Assessment of trabecular bone structure of the calcaneus using multi-detector CT: correlation with microCT and biomechanical testing. Bone. 2009; 44:976–83. [PubMed: 19442610]
13. Hildebrand T, Ruegsegger P. A new method for the model-independent assessment of thickness in three-dimension images. Journal of Microscopy. 1997; 185:67–75.
14. Saha PK, Wehrli FW. Measurement of trabecular bone thickness in the limited resolution regime of in vivo MRI by fuzzy distance transform. IEEE Transactions on Medical Imaging. 2004; 23:53–62. [PubMed: 14719687]
15. Vesterby A, et al. Star Volume of Marrow Space and Trabeculae of the First Lumbar Vertebra: Sampling Efficiency and Biological Variation. Bone. 1989; 10:7–13. [PubMed: 2660885]
16. Croucher PI, et al. Assessment of Cancellous Bone Structure: Comparison of Strut Analysis, Trabecular Bone Pattern Factor, and Marrow Space Star Volume. Journal of Bone and Mineral Research. 1996; 11:955–961. [PubMed: 8797116]
17. Vincent L. Efficient computation of various types of skeletons. presented at the SPIE San Jose, CA. 1991
18. Saha PK, et al. Volumetric topological analysis: a novel approach for trabecular bone classification on the continuum between plates and rods. IEEE Trans Med Imaging. 2010; 29:1821–38. [PubMed: 20562041]
19. Liu Y, et al. Quantitative Characterization of Trabecular Bone Micro-Architecture using Tensor Scale and Muti-Detector CT Imaging. presented at the MICCAI, Nice, France. 2012
20. Saha PK, et al. A new shape preserving parallel thinning algorithm for 3D digital images. Pattern Recognition. 1997; 30:1939–1955.

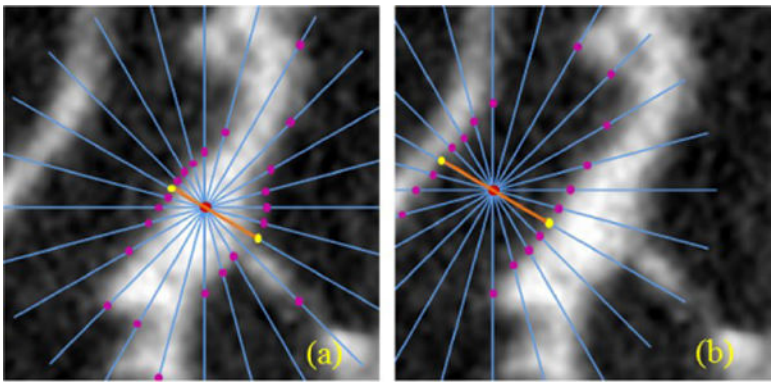

Figure 1.

Illustration of star line-based TB thickness and marrow spacing computation. (a) Candidate point (red), star lines (blue), edge locations (purple) and shortest intercept (orange) in TB thickness computation. (b) Same as (a) but for marrow spacing.

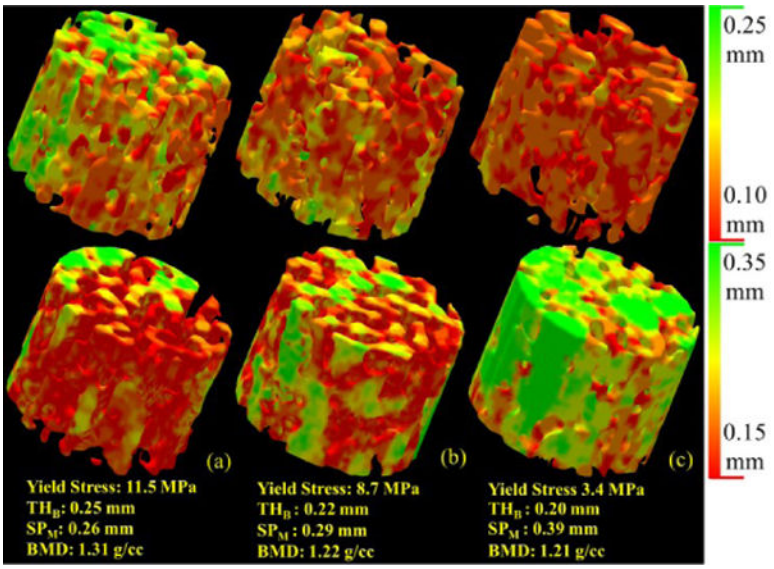

Figure 2.

Illustration of the TB thickness and marrow spacing measures for three different TB specimens – (a) strong (yield stress: 11.5 MPa), (b) moderate (7.1 MPa) and (c) weak (3.4 MPa).

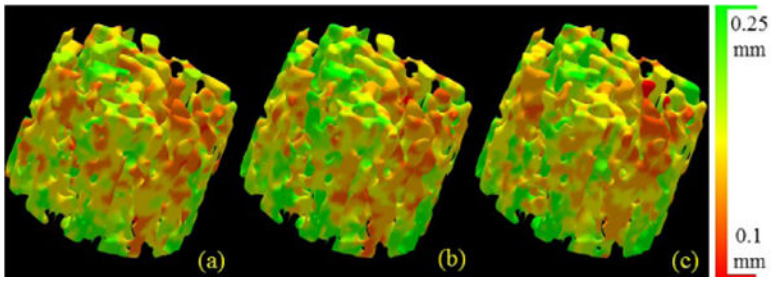

Figure 3.

Illustration of reproducibility of TB thickness measure under three repeat MD-CT scans (a–c). Specimens were repositioned on the CT table before each repeat scan.

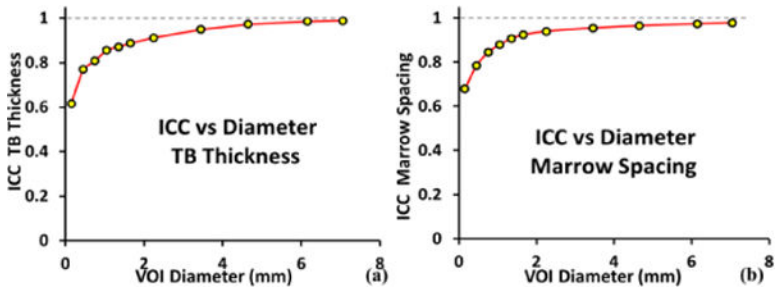

Figure 4.

Illustration of repeat MD-CT scan ICC values at different VOI diameters. At a VOI diameter of 3.45 mm or greater, the ICC value exceeded the mark of 0.95.

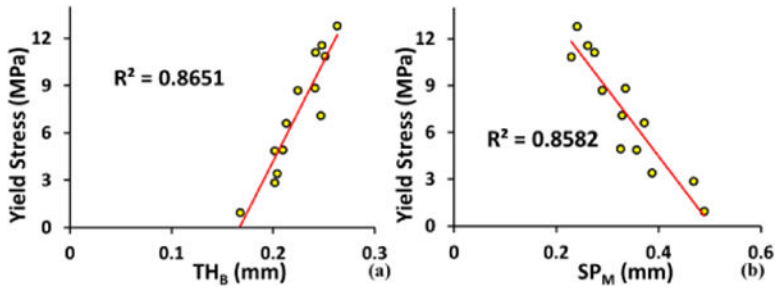

Figure 5.

Ability of different TB measures to predict bone strength shown in terms of R^2 values of linear correlation between yield stress and each of $\boldsymbol{TH_B}$ (a) and $\boldsymbol{SP_M}$ (b).